ISSN 2075-1133, Inorganic Materials: Applied Research, 2019, Vol. 10, No. 1, pp. 168–173. © Pleiades Publishing, Ltd., 2019.
Russian Text © I.G. Brodova, A.N. Petrova, S.V. Razorenov, E.V. Shorokhov, 2018, published in Materialovedenie, 2018, No. 7, pp. 3–8.

Interconnection of Structural Characteristics with Dynamic Properties of A5083 Aluminum Alloy

I. G. Brodova[a], A. N. Petrova[a, b, *], S. V. Razorenov[c, d], and E. V. Shorokhov[e]

[a] *Mikheev Institute of Metal Physics, Ural Branch, Russian Academy of Sciences, Yekaterinburg, Russia*
[b] *Ural Federal University, Yekaterinburg, Russia*
[c] *Institute of Problems of Chemical Physics, Chernogolovka, Russia*
[d] *National Research Tomsk State University, Tomsk, Russia*
[e] *Russian Federal Nuclear Center—All-Russian Research Institute of Technical Physics, Snezhinsk, Russia*
**e-mail: petrovanastya@yahoo.com*

Received October 31, 2017

Abstract—In this work, the resistance of high-strain rate deformation and fracture during shock-wave compression of aluminum alloy A5083 previously obtained in two structural states by torsion under high pressure or dynamic pressing is studied. It is shown by electron microscopy that sub-microcrystalline structures differ in the size of grain–subgrains, dislocation density, and ratio of low-angle and high-angle boundaries. It is established that, at the same grain size, the sub-microcrystalline alloy exhibits higher dynamic properties, and after dynamic pressing, it has higher spall strength.

Keywords: sub-microcrystalline structure, shock waves, high-rate deformation, strength
DOI: 10.1134/S2075113319010052

INTRODUCTION

Aluminum alloys are materials that, according to their purpose, are used in extreme conditions of operation. In this regard, the important issue remains the creation of an optimal set of mechanical and physical properties that ensure trouble-free operation of these materials. It is known that there is a direct relationship between the properties and structure of the alloys, which can vary widely, depending on the deformation-heat treatment. In recent years, promising research has been aimed at the development of various methods of megaplastic deformation (MPD), which ensure the refinement of the structure of alloys to submicro- and nanolevels [1, 2]. The creation of alloys with such a structural state led to the improvement of their properties under static loading conditions [3–6]; however, under the conditions of high-velocity deformation and shock-wave loading, this advantage over the coarse-crystalline state may not be maintained. The analysis of literature sources shows that the existing experimental data on the effect of the degree of structure refinement on the dynamic properties of materials are rather contradictory [7–9]. This is connected not so much with the nature of the materials and with the size of the structural components, but with their internal structure, the number and type of defects, and the ratio of low-angle and high-angle boundaries, i.e., with factors that are determined by the deformation mechanisms.

The purpose of this work is to determine the dynamic properties of a material with a different type of sub-microcrystalline structure and identify the general patterns and differences in the mechanical behavior of the A5083 aluminum alloy produced by various methods of severe plastic deformation using the example of an alloy of the same composition under shock-wave compression.

EXPERIMENTAL

The conventional alloy A5083 with the following chemical composition (wt %) was investigated: Al (base)–4.4 Mg–0.6 Mn–0.11 Si–0.23 Fe–0.03 Cr–0.02 Cu–0.06 Ti.

To obtain the samples with a sub-microcrystalline (SMC) structure, deformation methods which differ in the strain rate and loading scheme were used. An industrial hot-pressed alloy rod in the annealed condition with a hardness of HB = 75 served as a coarse crystalline analog. As a MPD method (deformation rate was 10^{-2} s^{-1}), high pressure torsion (HPT) of flat disks with a diameter of 20 and 1 mm thick was used. The number of revolutions of the anvil $n = 1, 5, 10$, which corresponded to the accumulated strain $e = 7.0, 8.6, 9.3$.

High-strain rate deformation of cylindrical samples with a diameter of 14 mm and length of 70 mm was carried out with one cycle of dynamic channel-angular pressing (DCAP) with a sample acceleration

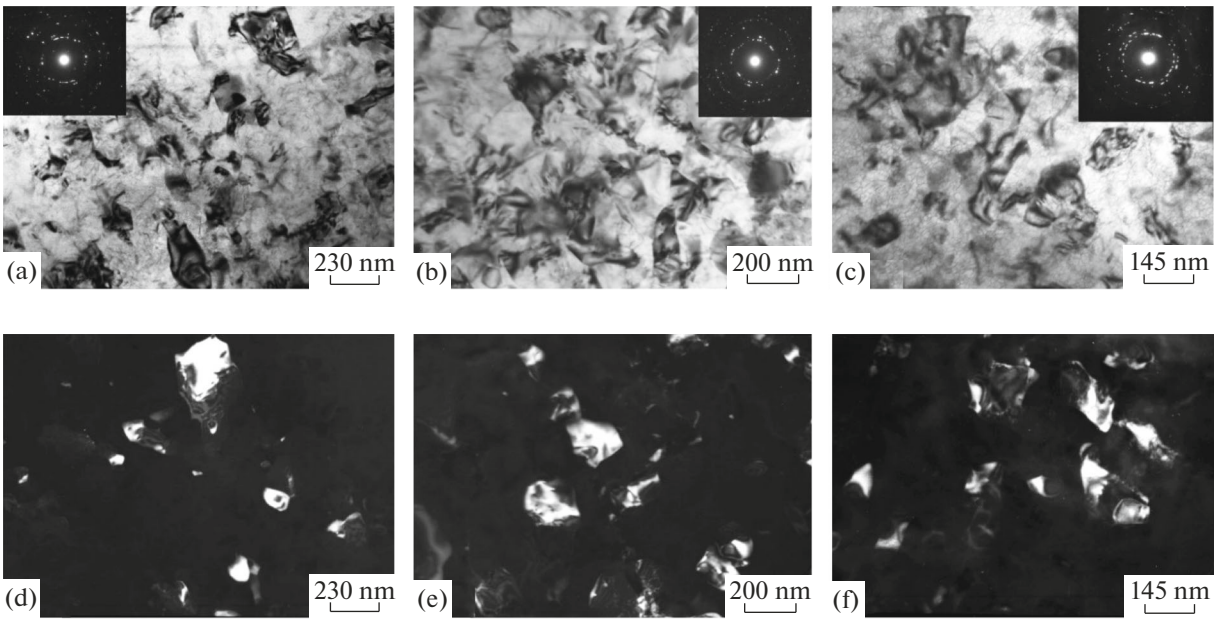

Fig. 1. Structure of alloy A5083 after HPT: (a, b, c) bright-field images with microdiffraction pattern; (d, e, f) dark-field images in matrix reflexes; (a, d) $e = 7.0$; (b, e) $e = 8.6$; (c, f) $e = 9.3$.

rate of 300 ms^{-1} (deformation rate was 10^5 s^{-1}). The main factor that distinguishes the DCAP experimental technique from other methods of deformation is the overlap of several deformation modes: compression–tension (due to the circulation of shock waves and rarefaction waves) and a simple shear.

In shock-wave experiments, disk-shaped samples were loaded by striking a flat aluminum plate, accelerated to 620 ± 30 ms^{-1} using an explosive device [10]. The rate of deformation before destruction varied from (1.6–2.0) × 10^5 to (3.5–4.7) × 10^5 s^{-1}, changing the thickness of the impactor. The pressure of shock-wave compression calculated using the shock adiabate of aluminum was 4 GPa. The mechanical characteristics of the alloy in the deformation process were determined from the free surface velocity profiles ($U_{fs}(t)$) recorded by a VISAR laser Doppler velocity meter. Calculations of the dynamic elastic limit σ_{HEL}, the dynamic yield strength Y, and the spall strength σ_{sp} were performed according to the formulas given in [10].

The structure of the samples after all types of processing was studied at different scale levels using a NEOPHOT-32 light optical microscope and a Philips CM-30 transmission electron microscope (TEM) at an accelerating voltage of 200 kV. A quantitative analysis of the size of structural components was performed via dark-field images using the Siams-700 computer program. X-ray diffraction analysis (XRD) was carried out on a DRON-3M X-ray diffractometer in CuK_α radiation. The dislocation density was estimated on the basis of data on the root-mean-square microstrain of the crystal lattice of the matrix and the size of the coherent-scattering regions. The microhardness of HV was determined on a PMT-3 device with a load of 0.2 N. The measurement error did not exceed 10%.

RESULTS AND DISCUSSION

Structure

The evolution of structure formation in the process of MPD depending on the number of revolutions of the anvil ($n = 1, 5, 10$) is considered; the real accumulated strain is $e = 7.00, 8.6, 9.3$. Figure 1 shows the stages of refinement of the initial coarse-crystalline (CC) structure to a sub-microcrystalline and nanocrystalline level.

As follows from the presented electron microscopic photographs, a strong structural refinement is observed already at an initial strain of $e = 7.0$ (see Figs. 1a, 1d). A fragmented structure is formed, the main part of which is occupied by deformed grains with an internal uneven contrast with diffuse high-angle boundaries, indicating a high level of internal stresses. With an increase in the degree of accumulated strain, the morphological features of structure formation are preserved, and the process of fragmentation is further developed. In the structure, predominantly high-angle boundaries are formed, as evidenced by the types of ring-like electron diffraction patterns with an increasing number of discretely located point spots, as well as the preservation of the deformational contrast inside the crystallites (see Figs. 1b, 1c, 1e, 1f). According to the results of the X-ray diffraction, it was established that, with an

increase in the accumulated strain in the material, the density of lattice dislocations increases from 7.8×10^{13} to 2.6×10^{14} m^{-2}. As defects accumulate, the dislocation ensemble changes as a whole, the interaction of dislocations is activated by low-angle boundaries, the disorientation of deformation boundaries increases, and mesodefects appear in triple junctions of grain boundaries—butt disclinations, and rotational modes of plasticity develop. These considerations are fully consistent with the physical concepts developed in [1, 2, 4, 11–15] and explain the process of microstructure refinement during MPD by the transformation of two types of boundaries of deformational nature.

The change in crystallite size depending on the magnitude of the accumulated strain was estimated from dark-field images using the Siams-700 program. According to the results of statistical analysis, histograms of the size distribution of crystallites were constructed and their average size was determined. A comparison of the histograms presented in Figs. 2a–2c, shows that, with increasing accumulated strain, the range of grain sizes narrows, and the proportion of large crystallites more than 450 nm in size decreases, i.e., the structure becomes more one-scale. The average size of grain-sub-grains of 170–180 nm at $e \le 8.6$ decreases to a nanolevel of 100 nm at $e = 9.3$ (Fig. 2c). The observed evolution of structure is in agreement with hardness data with increasing strain. Compared to the initial state, the hardness increases by 2.5 times, reaching 2500 MPa at $n = 10$. If we assume that the different mechanisms of hardening make their contributions additively, then the hardness of the deformed HPT alloy increases owing to the grain-boundary and dislocation components of hardening, since the process of HPT did not lead to the processes of deformation dissolution of intermetallic compounds or dynamic aging of the matrix.

During dynamic pressing of a coarse-crystalline alloy of the same composition, a SMC structure of a different type is formed. A typical picture of such a structure is shown in Figs. 3a and 3b. According to the results of TEM, in the sample of one cycle of pressing, mesostripes of shear separated by low-angle boundaries are formed. They have a width of 400–500 nm and are directed at an angle of 30°–45° to the direction of pressing (see Fig. 3a). The internal substructure (see Fig. 3a) was found inside the mesostripes on the dark-field images. Subgrains elongated along the mesoribbons are weakly oriented between each other, which indicates their deformation origin. Azimuth diffused reflections on the microdiffraction pattern (see Fig. 3a) indicate the predominant presence of low-angle misorientations. The average size of grains–subgrains determined via dark-field images was 240 nm. The shear mesobands parallel to each other pack together and form a band macrostructure consisting of fibers with the width of a few microns.

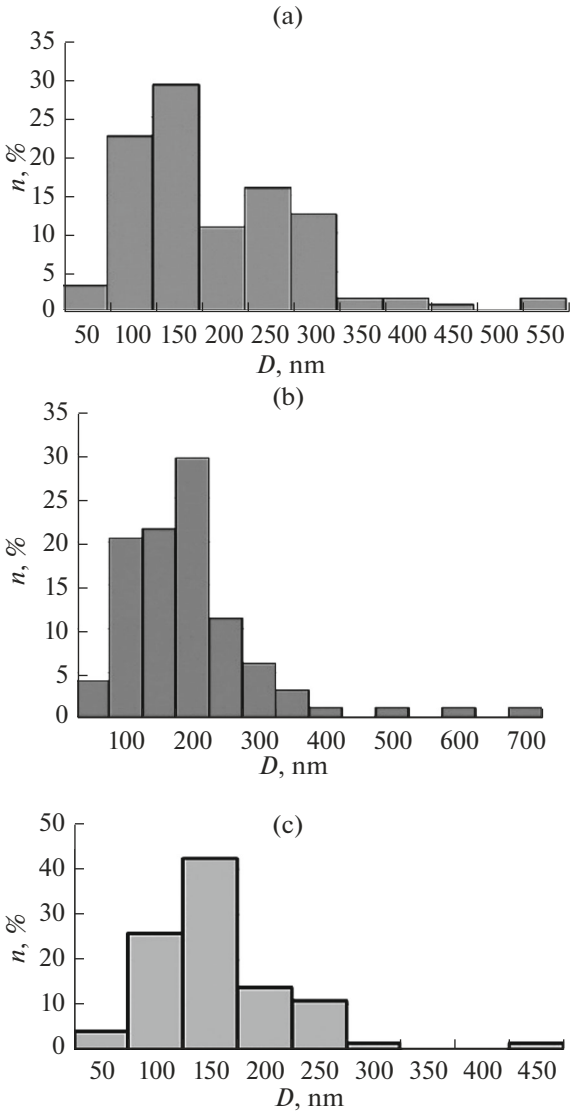

Fig. 2. Size distribution of fragments of structure: (a) $e = 7.0$; (b) $e = 8.6$; (c) $e = 9.3$.

The density of lattice dislocations according to XRD data is 8.7×10^{14} m^{-2}, which is higher than at HPT. Consequently, at the DCAP under high strain rate of 10^5 s^{-1}, a high density of dislocations is reached already after first cycle of DCAP owing to the increase in mobility of dislocations and activation of additional systems of sliding in fcc metals and alloys [16]. This result was previously repeated in the DCAP experiments of aluminum alloys of other compositions [10]. The experimentally detected features of structure formation during the DCAP of aluminum alloys are fully confirmed by simulating the process of SPD of metals using the system of equations for the mechanics of continuous media with defects [17], according to which under the action of a shock wave the density of dislocations increases and microscopic localization of plastic flow occurs in the shear bands [18].

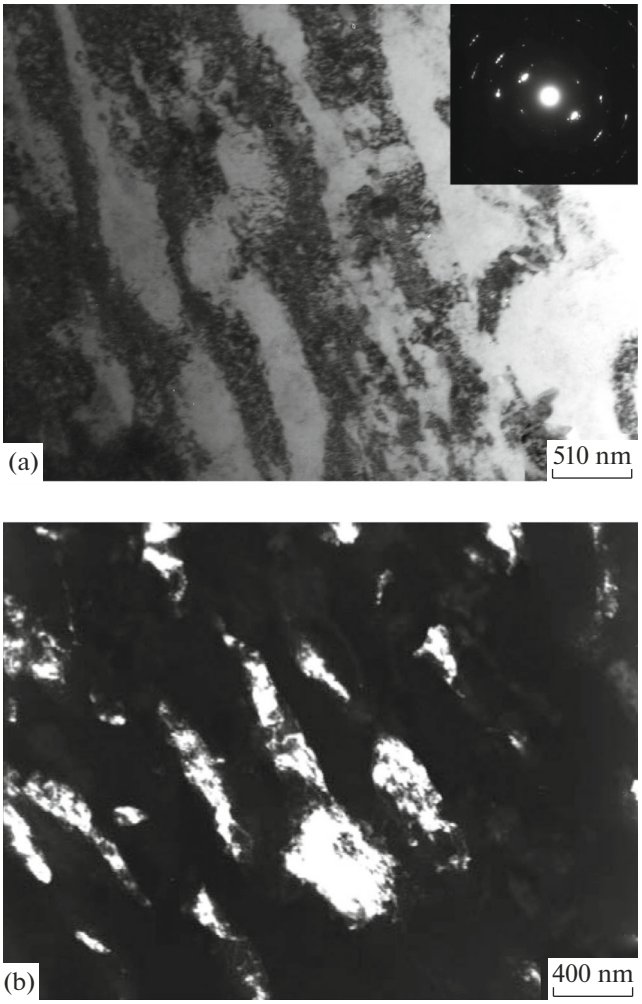

Fig. 3. Structure of alloy A5083 after one cycle of DCAP: (a) bright-field image with microdiffraction pattern; (b) dark-field image in matrix reflection.

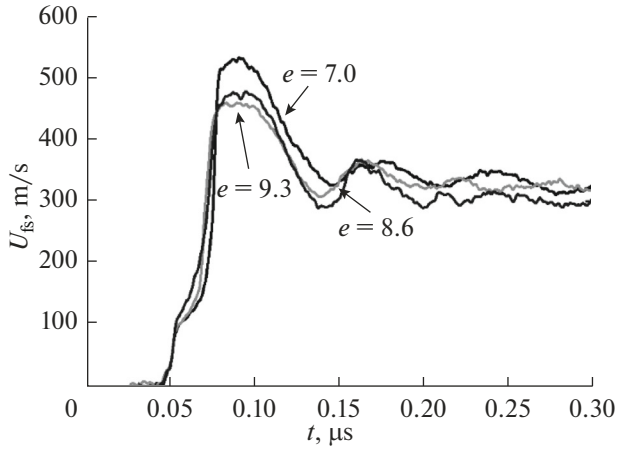

Fig. 4. Free surface velocity profiles of HPT samples obtained under shock compression with a rate of (3.5–4.7) × 10^5 s^{-1}.

The hardness of deformed DCAP A5083 alloy is equal to 1200 MPa. Taking into account the features of structure formation described above, it follows that the growth of hardening is reached mainly because of the defects of structure, dislocations, and high fraction of low-angle boundaries.

Thus, analyzing the experimental data described above, we can conclude that, using two methods of plastic deformation, HPT and DCAP, two different structural states were obtained in the same material, differing in the ratio of low-angle and high-angle boundaries, dislocation density grain size, and hardness.

Mechanical Properties under Shock Compression

The spall fracture of specimens previously obtained by HPT was investigated at two strain rates of (1.6–2.0) × 10^5 s^{-1} and (3.5–4.7) × 10^5 s^{-1}. Figure 4 shows the velocity profiles of HPT samples obtained in the process of shock compression at a strain rate of (3.5–4.7) × 10^5 s^{-1}, on which the exit to the surface of an elastic precursor of a plastic shock compression wave and parts of the next wave of a rarefaction is recorded. When a compression pulse is reflected from a free surface, tensile stresses arise, leading to spall fracture. These features are typical of the wave profiles recorded during the shock compression of aluminum alloys [7, 9, 10]. The dynamic characteristics of SMC and NC alloys obtained by HPT calculated from wave profiles in comparison with the CC analog are presented in the Table 1.

As can be seen from the presented data, an increase in the strain rate in the investigated range of loading parameters does not significantly affect the value of mechanical properties, and their difference can be attributed to experimental error.

As follows from Table 1, the values of the dynamic elastic limit and the dynamic yield strength of the SMC samples obtained by HPT are higher. For $n = 1$ and 5 ($e = 7.0$ and 8.6, respectively), the dynamic elastic limit and dynamic yield strength doubles in a comparison with the coarse-crystalline analog. Refinement of the structure to the nanoscale (at $n = 10$, $e = 9.3$) leads to an additional growth of σ_{HEL} and Y, approximately 10% more. Thus, the obtained values of σ_{HEL} and Y correlate with changes in the grain size. In contrast to this, the value of the critical breaking stress σ_{sp} is unambiguously unrelated to the scale of the structure obtained by the HPT.

The shock wave loading of the SMC samples previously obtained by the DCAP was realized at a strain rate of (1.6–2.0) × 10^5 s^{-1}. The results of this experiment are shown in Fig. 5. It has been established that, in the deformed state, the material also has enhanced dynamic properties relative to the CC analog, namely, $\sigma_{HEL} = 0.56$ Gpa and $Y = 0.31$ GPa, but the increase in these characteristics is less than only 1.5 times.

Table 1. Dynamic properties of alloy A5083 after HPT

Structure	n	e	σ_{HEL}, GPa	Y, GPa	σ_{sp}, GPa
SMC	1	7.0	0.76/0.77	0.41/0.42	1.53/1.13
SMC	5	8.6	0.77/0.78	0.42/0.43	1.16/1.18
NC	10	8.3	0.84/0.85	0.46/0.47	1.42/1.44
CC	–		–/0.37	–/0.19	–/1.52

In the numerator, the deformation rate was (3.5–4.7) × 10^5 s^{-1}, and in the denominator, the deformation rate was (1.6–2.0) × 10^5 s^{-1}.

Consequently, compared to the samples deformed by HPT, the samples after DCAP exhibit lower dynamic properties. The spall strength of the alloy after DCAP corresponds to the spall strength of the CC alloy and is 1.5 GPa. Judging by the amplitude and shape of the spall pulse, the rates of destruction of these materials are also close to each other.

To explain these results, we analyze the differences in the structure of alloys deformed by different methods. If we do not take into account the small difference in the average size of the structural components, namely, 240 nm for the SMC alloy obtained by DCAP and 200–150 nm for the SMC alloy after HPT (n = 1, 5), then the main factors for the difference are the ratio of low-angle and high-angle boundaries and the density of defects. Both of these factors contribute to the total hardening of the alloy and regulate the dynamic yield strength.

On the basis of certain values of Y, it follows that, despite the lower density of dislocations in the SMC structure after HPT, higher values of the yield strength (by 80 MPa) are achieved owing to the grain boundary hardening caused by the formation of a high fraction of grains with high-angle misorientation. The transition to a nanostructure at n = 10 and e = 9.3 and an increase in the length of nonequilibrium boundaries reinforce this difference up to 140 MPa, which also serves as proof of the correctness of the patterns found.

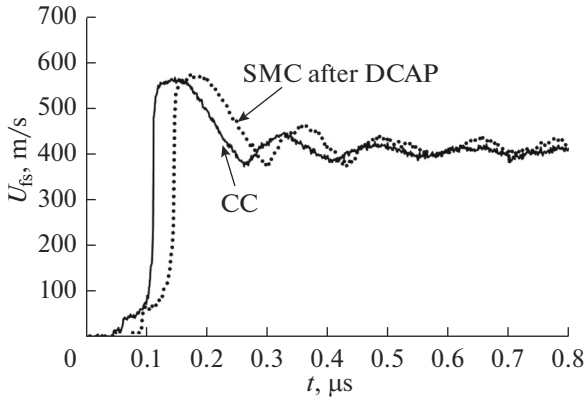

Fig. 5. Free surface velocity profiles of SMC sample after DCAP and coarse-crystalline sample obtained under shock-wave compression with a rate of (1.6–2) × 10^5 s^{-1}.

CONCLUSIONS

A comparison of the mechanical behavior under conditions of shock-wave compression of the SMC alloy A5083 obtained by HPT and DCAP has been carried out. On the basis of data of transmission microscopy and hardness, the main regularities of the formation of structural parameters (grain size, dislocation density, and ratio of low-angle and high-angle boundaries) are established depending on the speed and magnitude of the accumulated deformation, and the mechanisms of hardening of a material with different type of SMC structure are determined. It is shown that all the dynamic characteristics of the elastoplastic transition in the SMC states are 1.5–2 times higher than in the coarse-crystalline alloy. The highest spall strength is demonstrated by the SMC alloy obtained by DCAP, and the dynamic yield strength is higher in the SMC alloy obtained by HPT.

ACKNOWLEDGMENTS

Electron microscopy studies were carried out at the Center for Collective Use Testing Center of Nanotechnologies and Prospective Materials of the Institute of Metal Physics, Ural Branch, Russian Academy of Sciences. This work was carried out within a state task of FASO Russia (theme "Structure," no. 01201463331). Shock wave loading of samples and the analysis of their dynamic characteristics were performed under the partial financial support of Russian Foundation for Basic Research (project no. 18-03-00102) and the Program of Fundamental Investigations by the Presidium of the Russian Academy of Sciences no. 11P "Thermal Physics of High Energy Densities. Matter at High Pressures. Fundamental Problems of Plasma Confinement and Heating in Magnetic Traps."

REFERENCES

1. Langdon, T.G., The principles of grain refinement in equal-channel angular pressing, *Mater. Sci. Eng., A,* 2007, vol. 462, pp. 3–11.
2. Segal, V.M., Beyerlein, I.J., Tome, C.N., Chuvil'deev, V.N., and Kopylov, V.I., *Fundamentals and Engineering of Severe Plastic Deformation,* New York: Nova Science, 2010.
3. Markushev, M.V. and Murashkin, M.Yu., Mechanical properties of submicrocrystalline aluminum alloys after

severe plastic deformation by angular pressing, *Phys. Met. Metallogr.,* 2000, vol. 90, no. 5, pp. 506–515.

4. Estrin, Y. and Vinogradov, A., Extreme grain refinement by severe plastic deformation: a wealth of challenging science, *Acta Mater.,* 2013, vol. 61, pp. 782–817.
5. Shangina, D.V., Bochvar, N.R., and Dobatkin, S.V., Aging processes in low-alloy bronzes after equal-channel angular pressing, *Inorg. Mater.: Appl. Res.,* 2016, vol. 7, no. 4, pp. 465–470.
6. Aborkin, A.V., Babin, D.M., and Zakharov, A.A., The effect of the number of passes with equal channel angular pressing on the operational properties of aluminum alloy, *Materialovedenie,* 2013, no. 11, pp. 33–37.
7. Garkushin, G.V., Razorenov, S.V., and Kanel, G.I., Effect of structural factors on submicrosecond strength of D16T aluminum alloy, *Tech. Phys.,* 2008, vol. 53, no. 11, pp. 1441–1446.
8. Anis'kin, M.V., Ignatova, O.N., Kaganova, I.I., Kal'manov, A.V., Koshatova, E.V., Lebedev, A.I., Kosev, V.V., Podurets, A.M., Polyakov, L.V., Tkachenko, M.I., Tsibikov, A.N., Salishchev, G.A., Garkushin, G.A., Razorenov, S.V., and Zocher, M.A., Mechanical properties of tantalum during high-speed deformation, *Fiz. Mezomekh.*, 2010, vol. 13, no. 4, pp. 65–71.
9. Razorenov, S.V., Kanel, G.I., and Fortov, V.E., Submicrosecond strength of aluminum and an aluminum-magnesium alloy AMg6M at normal and enhanced temperatures, *Phys. Met. Metallogr.,* 2003, vol. 95, no. 1, pp. 86–91.
10. Brodova, I.G., Petrova, A.N., Razorenov, S.V., and Shorokhov, E.V., Resistance of submicrocrystalline aluminum alloys to high-rate deformation and fracture after dynamic channel angular pressing, *Phys. Met. Metallogr.,* 2015, vol. 116, no. 5, pp. 519–526.
11. Metlov, L.S., Glezer, A.M., and Varyukhin, V.N., Cyclic character of the evolution of the defect structure and the properties of metallic materials during megaplastic deformation, *Russ. Metall.* (Engl. Transl.), 2015, vol. 2015, no. 4, pp. 269–273.
12. Rybin, V.V., Zolotorevskii, N.Yu., and Ushanova, E.A., Fragmentation of crystals upon deformation twinning and dynamic recrystallization, *Phys. Met. Metallogr.,* 2015, vol. 116, no. 7, pp. 730–744.
13. Sarafanov, G.F. and Perevezentsev, V.N., Relaxation of the elastic field of a crystal during the subgrain boundary formation induced by plastic deformation, *Russ. Metall.* (Engl. Transl.), 2017, vol. 2017, no. 10, pp. 775–778.
14. Salishchev, G.A., Mironov, S.Yu., Zherebtsov, S.V., and Belyaev, A.N., Effect of deformation on misorientations of grain boundaries in metallic materials, *Mater. Phys. Mech.,* 2016, vol. 25, no. 1, pp. 42–48.
15. Perevezentsev, V.N., Svirina, Yu. V., and Kirikov, S.V., Simulation of dislocation structures formed during plastic deformation in elastic field of disclination under different conditions of dislocation generation, *Deform. Razrushenie Mater.,* 2017, no. 3, pp. 2–8.
16. Epshtein, G.N. and Kaibyshev, O.A., *Vysokoskorostnaya deformatsiya i struktura metallov* (High-Speed Deformation and Structure of Metals), Moscow: Metallurgiya, 1971.
17. Borodin, I.N. and Maier, A.E., Simulation of decay of shock waves in nanocrystalline metals, *Vestn. Chelyab. Gos. Univ., Fiz.*, 2011, vol. 38, no. 11, pp. 31–40.
18. Borodin, I.N. and Mayer, A.E., Localization of plastic flow at dynamic channel angular pressing, *Tech. Phys.*, 2013, vol. 58, no. 8, pp. 1159–1163.

Translated by A. Bannov